Research Square

Preprints are preliminary reports that have not undergone peer review.
They should not be considered conclusive, used to inform clinical practice,
or referenced by the media as validated information.

Assessment of IMD-HRRR Model in Predicting Extreme Rainfall Events over India

Akhil Srivastava

akhils.imd@gmail.com

India Meteorological Department

Prashant Kumar

Space Applications Centre

Raghu Nadimpalli

India Meteorological Department

Amit Kumar

India Meteorological Department

C. J. Johny

India Meteorological Department

Ananda K. Das

India Meteorological Department

P. K. Thapliyal

Space Applications Centre

Research Article

Keywords: Extreme rainfall events, IMD-HRRR, numerical weather prediction, GSMaP_ISRO, Extreme Dependency Score, India Meteorological Department, high spatial resolution, disaster management, CRA

Posted Date: November 10th, 2026

DOI: https://doi.org/10.21203/rs.3.rs-10736335/v1

License: This work is licensed under a Creative Commons Attribution 4.0 International License.
Read Full License

Additional Declarations: No competing interests reported.

Assessment of IMD-HRRR Model in Predicting Extreme Rainfall Events over India

Akhil Srivastava[1], Prashant Kumar[2], Raghu Nadimpalli[1], Amit Kumar[1], C. J. Johny[1], Ananda K. Das[1], and P. K. Thapliyal[2]

[1]India Meteorological Department, Ministry of Earth Sciences, New Delhi.

[2] Space Applications Centre, ISRO, Ahmedabad.

Corresponding author: Akhil Srivastava (akhils.imd@gmail.com)

Abstract

Climate vulnerability in India has intensified due to the increasing frequency of hydro-meteorological extreme rainfall events (EREs). While numerical weather prediction (NWP) models have improved for large-scale medium-range forecasting, precipitation forecasting, especially for extreme events, remains less reliable due to simplified representations of topography, land cover, and vegetation in global models. To address this, the India Meteorological Department (IMD) operates the High-Resolution Rapid Refresh (IMD-HRRR) model at 2 km horizontal resolution, assimilating hourly radar and surface observations to provide 12-hour nowcasts updated every 2 hours. This study evaluates the performance of the IMD-HRRR model in predicting extremely heavy rainfall events (≥204.4 mm/day) across mainland India in 2023. The IMD gauge-adjusted merged rainfall product GSMaP_ISRO (0.1° × 0.1°, hourly) was utilised to compare model forecasts using traditional metrics (bias, RMSE, correlation, and critical success index) and the Extreme Dependency Score (EDS), which is better suited for rare events. Results indicate that IMD-HRRR generally captures the spatial distribution of extreme rainfall over the Northwest, Northeast, and South Peninsular domains, with peak activity correctly predicted over Meghalaya, Assam, and the Western Ghats. However, systematic dry biases were observed across all domains (-0.61 to -0.93 mm/12 h), with higher root mean square deviation in the Northwest (~1.79 mm) and Northeast/South Peninsular regions (~3.54 mm). The model exhibits a slight dry bias over the Western Himalayas and Kutch, a wet bias over the Western Ghats, and an accurate representation of the Konkan–Karnataka coastal rainfall belt. EDS analysis confirms the model's ability to capture extreme events. The contiguous rain analysis (CRA)-based object verification shows efficient moisture convergence; however, it indicates shape & displacement errors for higher rainfall thresholds. Overall, IMD-HRRR provides valuable early warning guidance for extreme rainfall, though improvements to orographic and convective parameterisations are needed in mountainous regions.

Keywords: *Extreme rainfall events, IMD-HRRR, numerical weather prediction, GSMaP_ISRO, Extreme Dependency Score, India Meteorological Department, high spatial resolution, disaster management, CRA.*

1. Introduction

Climate vulnerability in India is a significant issue due to the increased frequency of hydro-meteorological extreme events throughout the year. In recent decades, there has been an increase in extreme rainfall events (EREs) linked to the monsoon, thunderstorms, and short-lived local cloudbursts across the subcontinent (Samantray et al. 2024), which typically last from a few hours to a few days. Predicting these high-impact weather events in near real-time is essential for proactive disaster management. During ERE, in a very short duration, conditions become particularly disastrous, leading to flash floods in urban areas (Nadimpalli et al. 2023). This intensification of rainfall has serious implications for flash floods, necessitating urgent adaptation measures for climate change (Fowler et al., 2021a, 2021b).

India has experienced an increase in the frequency and intensity of extreme monsoon rainfall over the past fifty years despite considerable interannual variability (IPCC, 6th Assessment Report, 2021). Current trends suggest that this increase will likely continue in the coming decades. The intensification of extreme sub-daily rainfall is attributed to convective feedback and changes in regional circulation, particularly in areas where temperatures surpass the Clausius-Clapeyron scaling, as observed in localised regions (Lenderink et al., 2017, 2021) and more extensive areas (Ali et al., 2021). Central India is particularly vulnerable to flash floods and landslides due to heavy rainfall events (Revadekar and Preethi, 2012). A threefold increase in rainfall extremes over central India from 1950 to 2015 highlights the enhanced variability of monsoon westerlies over the Arabian Sea (Roxy et al., 2017). Most rainfall occurs between June and September during the southwest monsoon season, and the climatic and topographical features of the subcontinent influence its rainfall (Osuri et al., 2020). The large-scale droughts and floods associated with the Indian summer monsoon negatively impact agricultural production and the economy on both geographical and temporal scales (Guhathakurta and Rajeevan, 2008; Naidu et al., 2015; Parthasarathy et al., 1994; Turner and Annamalai, 2012).

The accuracy of numerical weather prediction (NWP) models for large-scale, medium-range weather forecasting is moderate, but precipitation forecasting remains less reliable (Samantaray et al., 2024). Mesoscale models are driven by initial and boundary conditions provided by global models to achieve high spatial and temporal resolution in regional forecasts (Prasad et al., 2021). However, global models often overlook or simplify detailed topography, land cover, and vegetation. Both global and regional models tend to disregard these factors to enhance output quality. Several operational forecasting centres utilise mesoscale models to deliver comprehensive weather forecasts for specific geographical areas (Samantaray et al. 2024). These forecasts are fundamentally more predictable than those generated from synoptic flows, which depend on initialisation data, particularly when using the concept of terrain-forced circulation (Paegle and

Pielke et al., 1990). Radar analysis can also detect the characteristics of pre-monsoon convective rainfall (Das et al., 2015; Agnihotri et al., 2021; Kumar and Bhat, 2016).

In view of the above, the India Meteorological Department (IMD) operationally runs the High-Resolution Rapid Refresh (IMD-HRRR) model at a very high spatial resolution of 2 km, leveraging the advantages of radar data and surface observations (Srivastava et al., 2024). The details of the model are provided in the subsequent sections. The IMD-HRRR model provides the next 12-hour numerical guidance for precipitation and reflectivity every 2 hours. This model output is crucial for generating early warning indications for extreme rainfall events. Early warnings could help the authorities to take necessary measures to reduce damage to life and property. The present study aims to evaluate the performance of the IMD-HRRR model with respect to the prediction of extreme rainfall events that occurred during the year 2023 (January to December) over mainland India.

According to the IMD nomenclature (Table 1), rainfall of 6.45-11.55 cm/day at any location is classified as 'heavy rain'; 11.56-20.44 cm/day is considered 'very heavy'; and rainfall exceeding 20.44 cm/day is categorised as 'extremely heavy'. These extreme events are rare and severe, causing significant socio-economic impacts due to the damage they inflict on life and property. Historical records indicate increased frequency and intensity of these extreme rainfall events (Roy and Balling, 2004; Goswami et al., 2006).

Table 1: IMD Nomenclature of rainfall intensity for any station over India

Very Light to Light Rainfall	0.1-15.5 mm
Moderate Rainfall	15.6-64.4 mm
Heavy Rainfall	64.5-115.5
Very Heavy Rainfall	115.6-204.4
Extremely heavy Rainfall	>= 204.4

The forecast accuracy of NWP models has steadily improved over the past couple of decades, as demonstrated by numerous studies (Kalnay et al., 1998; Vitart, 2013; Magnusson and Kallen, 2013; Walters et al., 2014). Recent studies have also reported on the verification of rainfall forecasts over India (Mandal et al., 2007; Das et al., 2008; Ashrit and Saji, 2010; Durai and Bharadwaj, 2013; Ashrit et al., 2015; Sharma et al., 2017; Osuri et al., 2020). Most of the previous studies employed standard verification metrics, including correlation coefficient (CC), Root Mean

Squared Error (RMSE), Probability of Detection (POD), False Alarm Ratio (FAR), Threat Score (TS), and Equitable Threat Score (ETS), which are well-established and widely used in the literature. However, most of these standard metrics are not adequate for assessing rare and extreme events, as their values tend to become exceedingly low (Stephenson et al., 2008). Verifying extreme rainfall events becomes even more challenging, as they are rare, isolated events that occur in isolated places and often go unreported. Events like cloudbursts or mini cloudbursts happen mostly over hilly terrain.

This study presents rainfall verification over mainland India at a 2 km horizontal resolution from the IMD-HRRR model, using traditional verification scores such as bias, RMSE, and correlation for extreme rainfall events. Additionally, the statistical challenges related to verifying extreme events are addressed using the EDS score. The performance of the IMD-HRRR model is also briefly reviewed with respect to terrain height in the evaluation of extreme rainfall amounts.

2. Data and methodology

2.1. Case studies for ERE

The frequency of extreme rainfall events (ERE) linked to the monsoon, thunderstorms, and short-duration local cloudbursts, typically lasting from a few hours to a few days, has risen in recent decades across the subcontinent (Samantray et al. 2024). Operational numerical weather prediction (NWP) models often lack sufficient accuracy when it comes to forecasting precipitation, particularly in the case of heavy rainfall events (Wang and Yuan 2018; Siddique et al. 2015). The IMD-HRRR model is implemented to provide objective guidance for high-intensity events for early preventive action. The high-impact rainfall event occurring in a very short timeframe is intended to be forecast by the IMD-HRRR model. Therefore, in this paper, all the extremely heavy rainfall cases (daily rainfall exceeding 20 cm) in 2023 are considered for verification with respect to the IMD-HRRR forecast. The details of extremely heavy rainfall cases in different meteorological subdivisions of India considered in this study are given in Table 1 below.

Table 1: List of extremely heavy rainfall cases in India in 2023

Meteorological subdivision	Dates
Arunachal Pradesh	29th July
Assam & Meghalaya	14th June, 15th June, 16th June, 17th June, 18th June, 19th June, 21st June, 22nd June, 01st July, 02nd July, 03rd July, 12th July, 13th July, 06th August, 07th August, 09th August, 13th August, 23rd August, 27th August, 07th October, 08th October

Sub-Himalayan West Bengal & Sikkim	18th June, 19th June, 21st June, 28th June, 2nd July, 13th July, 23rd August, 25th August, 28th August, 29th August
Gangetic West Bengal	28th June, 4th October
Odisha	16th July, 18th July, 01st August, 02nd August, 12th September, 14th September
Bihar	12th July, 14th July, 09th August, 10th August, 23rd September, 24th September
East Uttar Pradesh	1st July, 12th July, 23rd August, 11th September, 12th September
West Uttar Pradesh	22nd June, 25th June, 11th July, 13th July, 27th July, 11th September, 17th September, 23rd September
Uttarakhand	11th July, 13th July, 18th July, 9th August
Haryana, Chandigarh & Delhi	9th July, 10th July, 11th July, 11th August
Punjab	9th July, 10th July
Himachal Pradesh	9th July, 10th July, 11th July, 14th August, 23rd August
Jammu & Kashmir & Ladakh	9th July, 19th July
West Rajasthan	18th June, 19th June, 27th July
East Rajasthan	18th June, 19th June, 10th July, 10th September, 17th September, 18th September
West Madhya Pradesh	13th July, 4th August, 16th September, 17th September
East Madhya Pradesh	28th June, 29th June, 3rd August, 4th August, 15th September
Gujarat Region	18th June, 30th June, 1st July, 2nd July, 19th July, 20th July, 22nd July, 23rd July, 27th July, 28th July, 29th July, 17th September, 18th September
Saurashtra & Kutch	17th June, 30th June, 1st July, 19th July, 20th July, 21st July, 22nd July, 23rd July, 19th September
Konkan & Goa	29th June, 05th July, 18th July, 19th July, 20th July, 21st July, 26th July, 27th July, 28th July, 08th September, 09th September

Madhya Maharashtra	18th July, 19th July, 20th July, 23rd July, 28th July
Marathawada	21st July, 28th July
Vidarbha	22nd July
Chhattisgarh	27th June, 27th July, 03rd August
Coastal Andhra Pradesh & Yanam	05th December, 06th December
Telangana	20th July, 22nd July, 25th July, 27th July, 28th July, 06th December
Rayalaseema	5th December
Tamil Nadu, Puducherry & Karaikal	13th July, 25th July, 09th November, 23rd November, 04th December, 05th December, 18th December, 19th December, 30th December
Coastal Karnataka	6th July, 19th July, 22nd July, 23rd July, 26th July
South Interior Karnataka	7th July, 23rd July
Kerala & Mahe	6th July, 15th October

2.2. GSMaP_ISRO rainfall

The reference rainfall for this study is taken from GSMaP_ISRO. The GSMaP_ISRO is a precipitation product developed through the collaboration between the Indian Space Research Organisation (ISRO) and the Japan Aerospace Exploration Agency (JAXA) under the Implementation Agreement (IA), specifically tailored for the Indian subcontinent. This product has been available from March 2000 onwards. This dataset offers a horizontal resolution of 0.1° x 0.1° on a latitude/longitude grid with an hourly temporal resolution. It is based on the Global Satellite Mapping of Precipitation (GSMaP) algorithm (Kubota et al., 2020; Kumar et al., 2021, 2022), with gauge correction from the IMD, making it a specialised product focused on the Indian landmass. The GSMaP algorithm, developed by JAXA, provides a comprehensive view of precipitation using data from microwave radiometers and cloud-motion information from geostationary infrared (IR) technology. The algorithm is divided into three key categories for precise measurement: microwave imager, microwave sounder, and microwave-infrared (MVK) combination (Mega et al., 2019). A detailed evaluation of GSMaP_ISRO during the Indian summer monsoon seasons from 2000 to 2020, comparing it with ground-based, satellite-based, and various merged rainfall products, is provided by Kumar et al. (2022).

2.3. *IMD-HRRR rainfall forecast*

The IMD-HRRR model is the numerical modelling system implemented in the IMD in 2021 to provide real-time operational numerical guidance to forecasters targeting nowcast to very short-range forecasts (Srivastava et al. 2024). The IMD-HRRR model is a 2 km horizontal resolution model based on the WRF ARW core with WRFDA data assimilation, ingesting the radar data and surface observations every hour. The model is initialised every hour and provides the forecast for the next 12 hours, updated every 2 hours. Therefore, the IMD-HRRR forecast of precipitation for the next 12 hours, updated every 2 hours, is considered for verification in this study. The IMD-HRRR model runs in parallel for 3 different domains covering mainland India. There are the northwest HRRR_NW, northeast HRRR_NE, and south peninsular HRRR_SP domains. These domains are shown in Fig. 1.

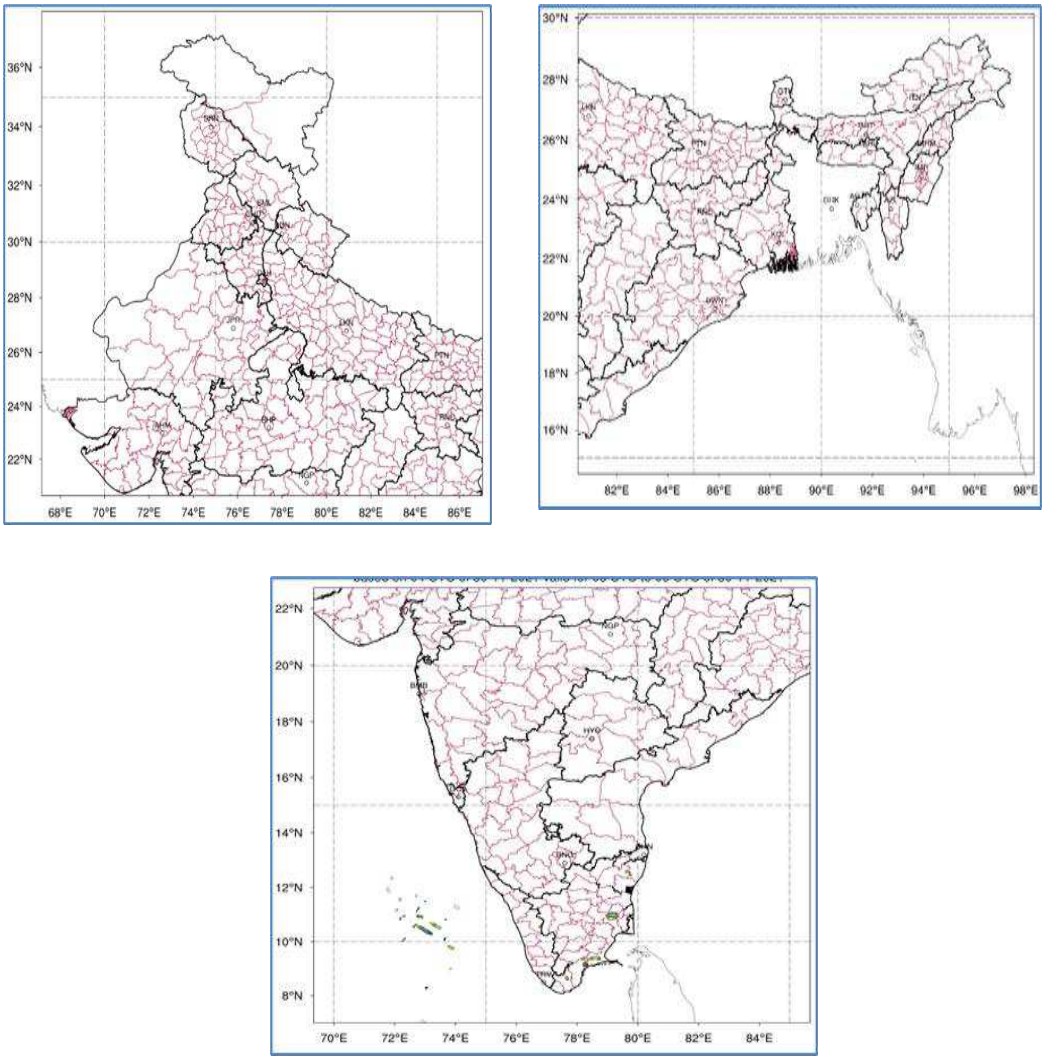


Fig. 1. Domains of the IMD-HRRR model.

The schematic diagram of the real-time IMD-HRRR model operationally run at IMD is shown in Fig. 2. The other details of the model can be seen in Srivastava et al. (2024).

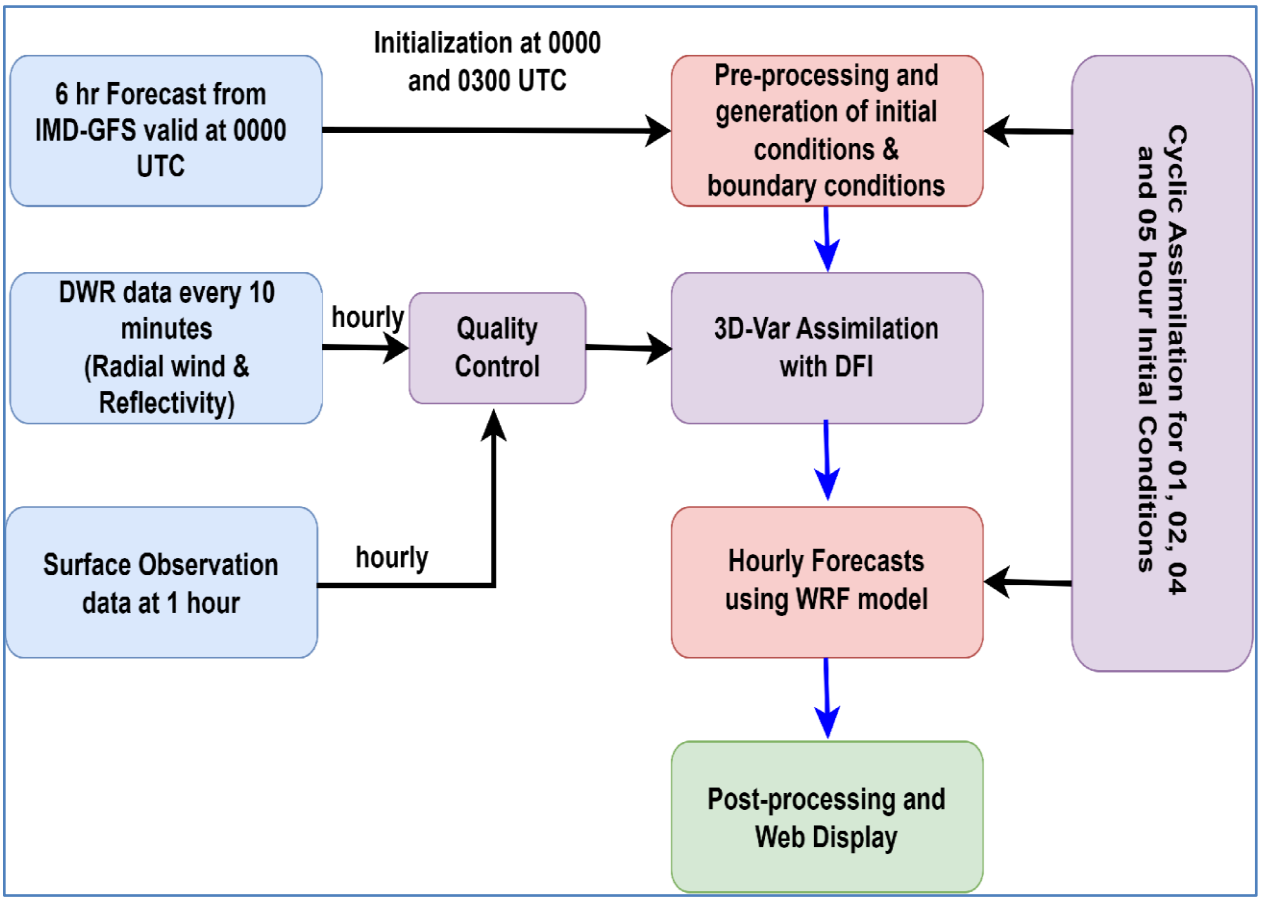


Fig. 2. The schematic diagram of the Operational IMD-HRRR model

The IMD-HRRR rainfall forecast is available for the next 12 hours after every 2 hours. So, all the forecast cycles of the IMD-HRRR model falling on the dates of extremely heavy rainfall, as per Table 1, are considered for verification. The spatial distribution of rainfall from the IMD-HRRR model for the 12-hour forecast after every 2 hours and rainfall in the corresponding 12 hours in GSMaP_ISRO are provided to give an overall scenario of observed and predicted rainfall over three domains of the IMD-HRRR model over mainland India.

2.4. Model rainfall forecast verification over India

In this study, categorical verification is employed based on the components of the contingency table (Table 2) analysis. The Critical Success Index (CSI), or Threat Score, is calculated for different rainfall thresholds for the three IMD-HRRR domains of NW, NE, and SP India. The CSI is determined by the formula a / (a + b + c), where "a" represents hits, "b" represents false alarms,

and "c" represents misses. The CSI ranges from 0 to 1, with a perfect score being 1. Jolliffe and Stephenson (2011) and Wilks (2011) comprehensively describe these scores.

Table 2: Contingency Table

Forecast	**Observed**		
	Yes	**No**	**Total**
Yes	Hits(a)	False Alarms (b)	Forecast Yes
No	Misses(c)	Correct Negatives (d)	Forecast No
Total	**Observed: Yes**	**Observed No**	**Total**

The study also reveals the bias, root mean square deviation, and correlation between the observed and forecasted rainfall for the three domains of IMD-HRRR. It is known that extreme rainfall activities are also supported by the orographic features. Most cloud bursts and similar intense events are reported from the mountainous regions. Therefore, in this study, the rainfall forecast for these extremely heavy rainfall days is also verified for different terrain heights to assess the performance of the IMD-HRRR model for these difficult-to-predict scenarios.

As the rainfall amount realised in a day increases, simultaneously, its occurrence in nature also decreases. In general, the extremely heavy rainfall events for a location are fewer than the moderate to heavy rainfall events. Therefore, these event numbers are mostly inadequate when traditional metrics like the Probability of Detection (POD), False Alarm Rate (FAR), or Critical Success Index (CSI) are considered based on a contingency table approach. As an additional verification metric, the Extreme Dependency Score (EDS) is designed to assess forecasts' accuracy for rare or extreme events. It evaluates the correlation between forecasted and observed extremes, especially in cases where traditional metrics like POD or FAR may fall short due to the infrequency of the event. EDS addresses the issue of low event occurrence rates, ensuring forecast performance is neither exaggerated nor diminished for extreme events. The score ranges from -1 to 1, with values near 1 indicating strong agreement between forecasts and observations of extremes and values near -1 reflecting poor forecast performance. This metric is especially valuable in forecasting rare meteorological events such as extreme rainfall, severe storms, or tropical cyclone landfalls, where accurate extreme event predictions are critical for effective disaster response (Jolliffe and Stephenson 2011; Wilks 2011). Therefore, in this study, the EDS scores for different thresholds of rainfall are verified for the three domains of the IMD-HRRR model.

In addition to the above, the Contiguous Rain Analysis (often referred to in spatial verification as Contiguous Object-Based Analysis or contiguous rain area methods, like CRA) represents a major shift from traditional point-by-point forecast verification to a spatial, feature-oriented approach. Older metrics like RMSE, Threat Score, and Equitable Threat Score all work the same way: grid point against grid point, pixel against pixel. These scores particularly have limitations with high-resolution models, where a forecast can get the rainfall shape and intensity almost right while still scoring poorly just because it shifts a few kilometres off – the so-called double penalty problem.

CRA resolves it by considering rain as a cohesive, distinct object in place of a scatter of unrelated points. It then tries to bring out the total forecast errors into physically meaningful pieces. In this process, a threshold (> 5 mm/12 hr, > 10 mm/12 hr, etc.) is applied to the spatial domain, and it continuously traces out every spot where that threshold is exceeded continuously across the map. This process is followed for both the observation and the forecast to generate two sets of objects for comparison. From there, the forecast object is shifted in latitude and longitude until it maximises the correlation between the two fields or minimises the mean squared error. After the best-fit position is found, the leftover error inside the object splits into three components, each one providing information about where the forecast actually went wrong.

Total Error = Displacement Error + Volume Error + Pattern Error

The displacement error is what corrects for when the forecast object gets shifted to its best-fit position. It indicates timing or speed issues in the model's dynamics, like a weather system moving too slowly as compared to observation. Volume error comes from a mismatch in total rainfall between forecast and observation, usually pointing to a mismatch in moisture convergence or the microphysics scheme. The residual error after displacement and volume error is the pattern error. It reflects the model's failure to capture fine-scale structure, gradients, and the exact alignment of convective cells within the rain area. CRA doesn't just flag that a forecast was wrong; it explains why: where the model put the rain (displacement), how much it produced (volume), and what it looked like once those two are accounted for (pattern).

3. Results and discussion

Figure 3 lays out the spatial patterns of 12-hour accumulated rainfall, comparing IMD-HRRR forecasts against GSMaP-ISRO observations across the NW, NE, and SP domains. This is the mean rainfall for each 12-hour window corresponding to the model's forecast cycle, considering all extremely heavy rainfall days in 2023 across the three regions. Figure 4 shows the corresponding bias and RMSD, and together they point to systematic errors in the HRRR forecasts. Both datasets pick up strong rainfall gradients, but HRRR consistently underestimates the heaviest rainfall cores even as it maintains good spatial agreement with what was actually observed. In the NW domain (a, b), both GSMaP and IMD-HRRR show high rainfall (>30 mm) concentrated in

the northern and central parts, with a strong north-south gradient.

The IMD-HRRR forecast captures the overall spatial structure but shows reduced intensity in the peak rainfall areas, with maximum values around 25-30 mm compared to observed values exceeding 35 mm. The NE domain (c, d) exhibits more scattered and lower-intensity rainfall across the region, with isolated pockets of 20-30 mm in the central and eastern areas. IMD-HRRR reproduces this patchy structure reasonably well, though it appears to slightly overpredict in some isolated locations while maintaining the overall spatial distribution. The SP domain (e, f) shows the most intense and spatially extensive rainfall, with a broad swath of 20-30 mm stretching across the central region and heavier cores (>35 mm) in the southeast. IMD-HRRR captures the large-scale pattern but underestimates the heaviest rainfall, with forecast maxima around 25-30 mm where observations exceed 35 mm. In general, the observed rainfall shows that short and intense rainfall spells were mainly concentrated over the Assam & Meghalaya region of Northeast India & the Western Ghats region of South Peninsular India compared to other regions on the extremely heavy rainfall days in 2023. The spatial verification demonstrates that IMD-HRRR successfully captures the large-scale rainfall distribution across all three domains during this extreme event.

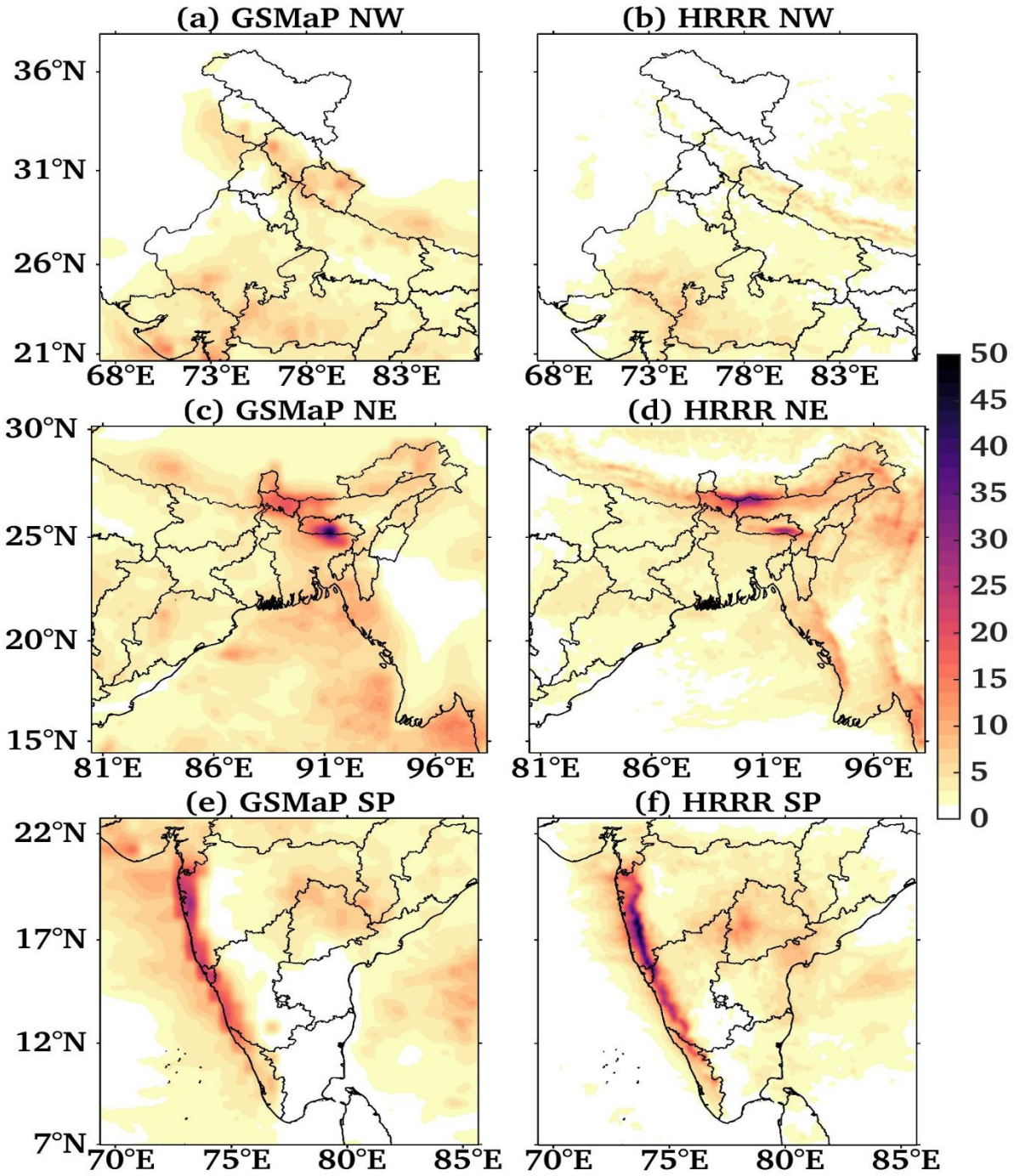


Fig. 3. The 12-hour mean rainfall (mm) from IMD-HRRR & GSMaP_ISRO for all extremely heavy rainfall days in 2023 in three IMD-HRRR domains of NW, NE & SP India.

In the NW India domain, the IMD-HRRR model captured the relative spatial intensity of rainfall over different regions of NW India, along with a slight dry bias over the Western Himalayan Region and extreme Kutch during extreme rainfall days of 2023. The IMD-HRRR model captured the peak mean rainfall activity over south Meghalaya and Northwest Assam & neighbourhood in

the NE India domain. The model in the NE domain also shows a slight dry bias over northern & eastern parts of the Bay of Bengal and a wet bias over Myanmar. In the SP India domain, the IMD-HRRR model predicted a belt of extreme rainfall activity along the west coast (Konkan coast to Karnataka coast). The IMD-HRRR model showed a wet bias over the Western Ghats and a dry bias over the adjoining Arabian Sea. In general, the other regions of mainland India didn't show any significant bias.

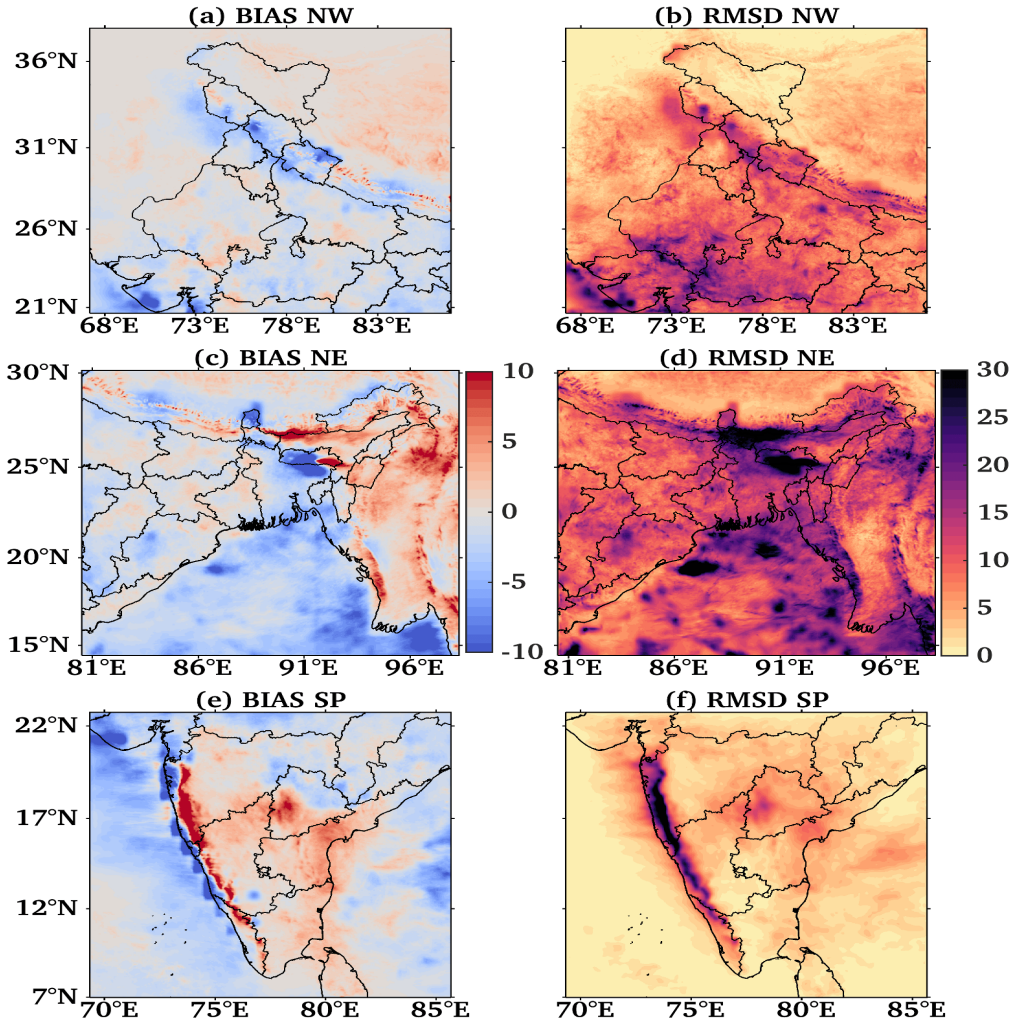


Fig. 4. The bias and RMSD in the 12-hour rainfall forecast from IMD-HRRR as compared to GSMaP_ISRO for all extremely heavy rainfall days of 2023 in three IMD-HRRR domains of NW, NE & SP India.

The RMSDs for different domains are shown in Fig. 4. The RMSD provides a comprehensive view of the magnitude of errors in a prediction model, combining both the variance and bias into a single number. Figure 4 shows that the RMSD is on the higher side in the northwest and northeast regions, whereas the RMSD is less prevalent over the south peninsular domain.

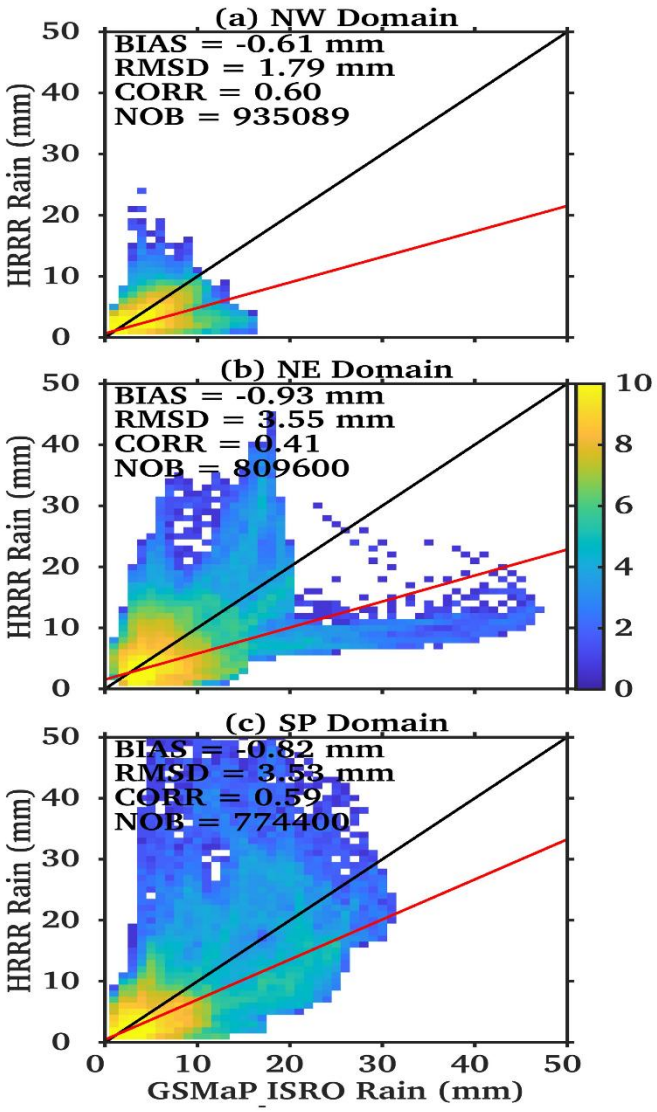


Fig. 5. The bias and RMSD for the three domains of the IMD-HRRR model for 12 hours

Fig. 5 compares HRRR rain forecasts against GSMaP ISRO rainfall for the NW, NE, and SP domains using density scatter plots. The density scatter plots of HRRR rainfall against GSMaP-ISRO rainfall indicate a generally positive relationship in all three domains, but with clear systematic underestimation at higher rainfall amounts. It indicates that most of the short and intense rainfall events occurred over northeast and south peninsular India compared to northwest India. The dry bias is seen over the three domains, ranging from -0.61 mm/12 hours over NW India, -0.93 mm/12 hours in NE India and -0.82 mm/12 hours in SP India, and RMSD is of the order of 1.79 mm/12 hours over the NW India domain, 3.55 mm/12 hours and 3.53 mm/12 hours over the northeast and south peninsular domains, respectively. Across all three domains, the negative bias values indicate that HRRR tends to underpredict rainfall, especially for larger GSMaP-observed amounts. The NW domain performs best in terms of lowest error and highest correlation, while the NE domain shows the weakest relationship between forecast and observed

rainfall. Overall, the plots show systematic underestimation at higher observed rainfall amounts, with the forecast clustered more strongly at lower-to-moderate values than the 1:1 line suggests.

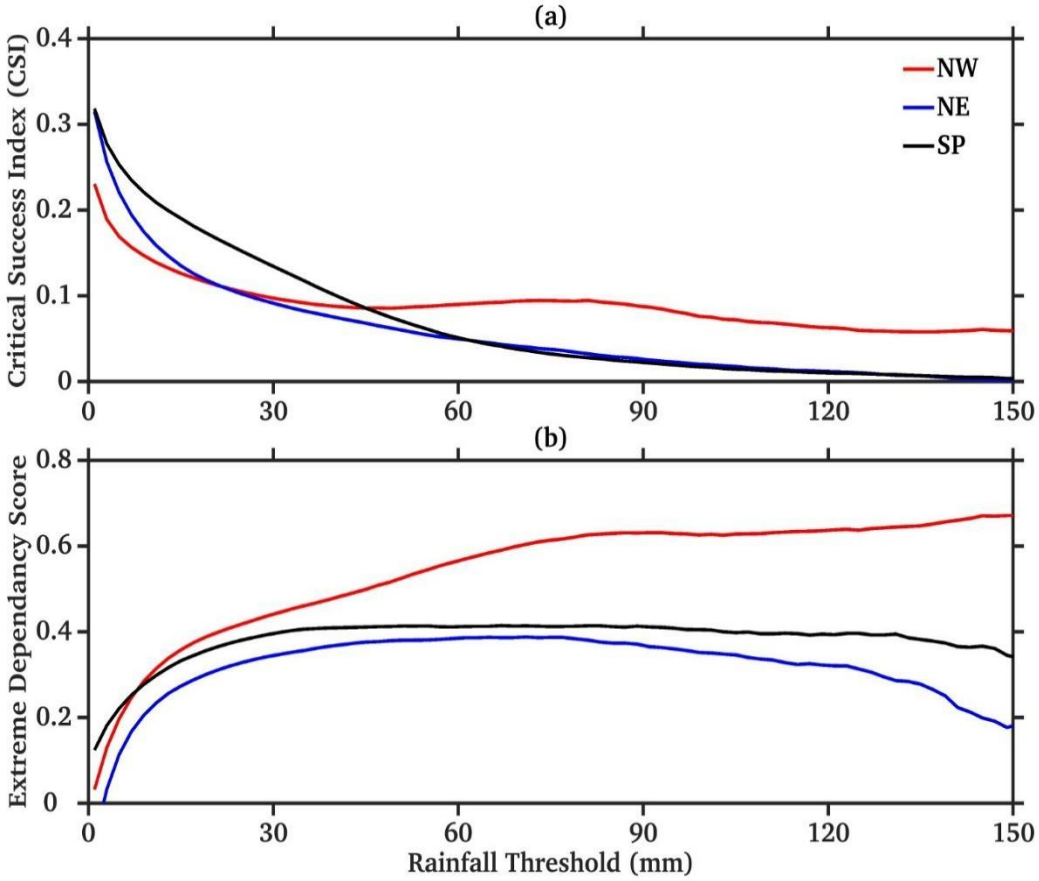


Fig. 6. The Critical Success Index and Extreme Dependency Scores for different rainfall thresholds in 12 hours

Figure 6 breaks down forecast skill by rainfall threshold for the three regions — **NW, NE, and SP**. Panel (a) shows the CSI, which drops off as the threshold increases, across all three domains. Panel (b) shows the Extreme Dependency Score (EDS) – it moves fast at low thresholds, then levels out or slowly reduces once the rainfall threshold increases. CSI for the SP domain starts on top and remains higher than the CSI for the other domains till the rainfall mid-range thresholds; then it decays steadily toward near zero as thresholds increase. NE also starts at a higher position than the NW domain but rapidly reduces at higher rainfall thresholds. CSI for the NW domain starts at the lowest level compared to the other two domains but doesn't reduce rapidly and stays steady at higher rainfall thresholds. This indicates better retention skill for heavy rainfall events in the NW domain as compared to the NE & SP domains.

With EDS, the IMD-HRRR model performs moderately well for the SP region. It rises rapidly at lower rainfall thresholds and stabilises around 0.4 before slightly decreasing at the higher threshold. The EDS shows relatively poorer skill, reaching its maximum value somewhere in the middle thresholds and then reducing rapidly for higher rainfall amounts. The northwest region displays the strongest and most persistent performance. The EDS values increase rapidly for the NW region and show the highest values among the three regions. Fig. 6 displays how the relative forecast skill for extreme rainfall changes with threshold across NW, NE, and SP. In panel (a), CSI reduces as the threshold rises for all three regions, and skill drops as events get more extreme. The SP region shows the highest CSI at low-to-moderate thresholds, whereas the CSI for the NW region stays comparatively steadier at higher thresholds, and the NE region shows the sharpest reduction at the large thresholds. In panel (b), EDS increases rapidly at lower thresholds and then levels off, with NW showing the strongest performance for high rainfall thresholds, SP remaining moderate, and NE weakening noticeably beyond about 100 mm. Overall, the verification suggests that the forecast performs better for moderate rainfall than for the most intense events, but NW retains the best extreme-rainfall discrimination among the three regions.

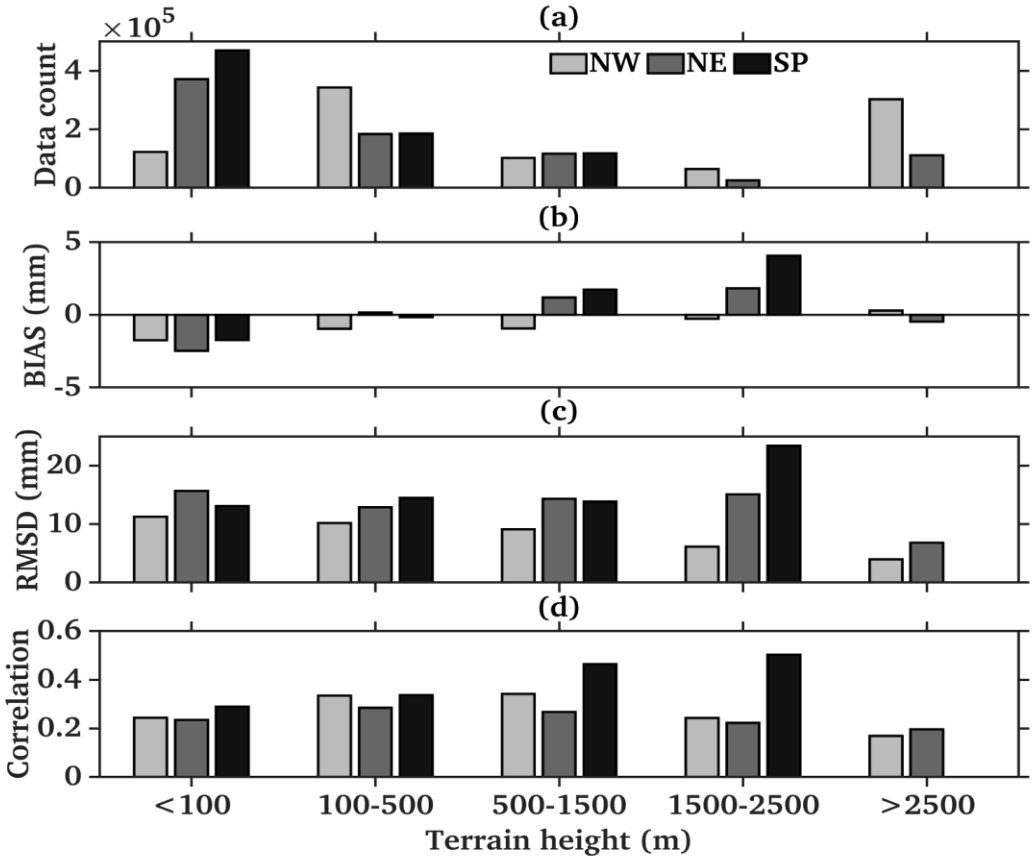


Fig. 7. Terrain-wise IMD-HRRR model rainfall forecast performance for rainfall in 12-hour intervals.

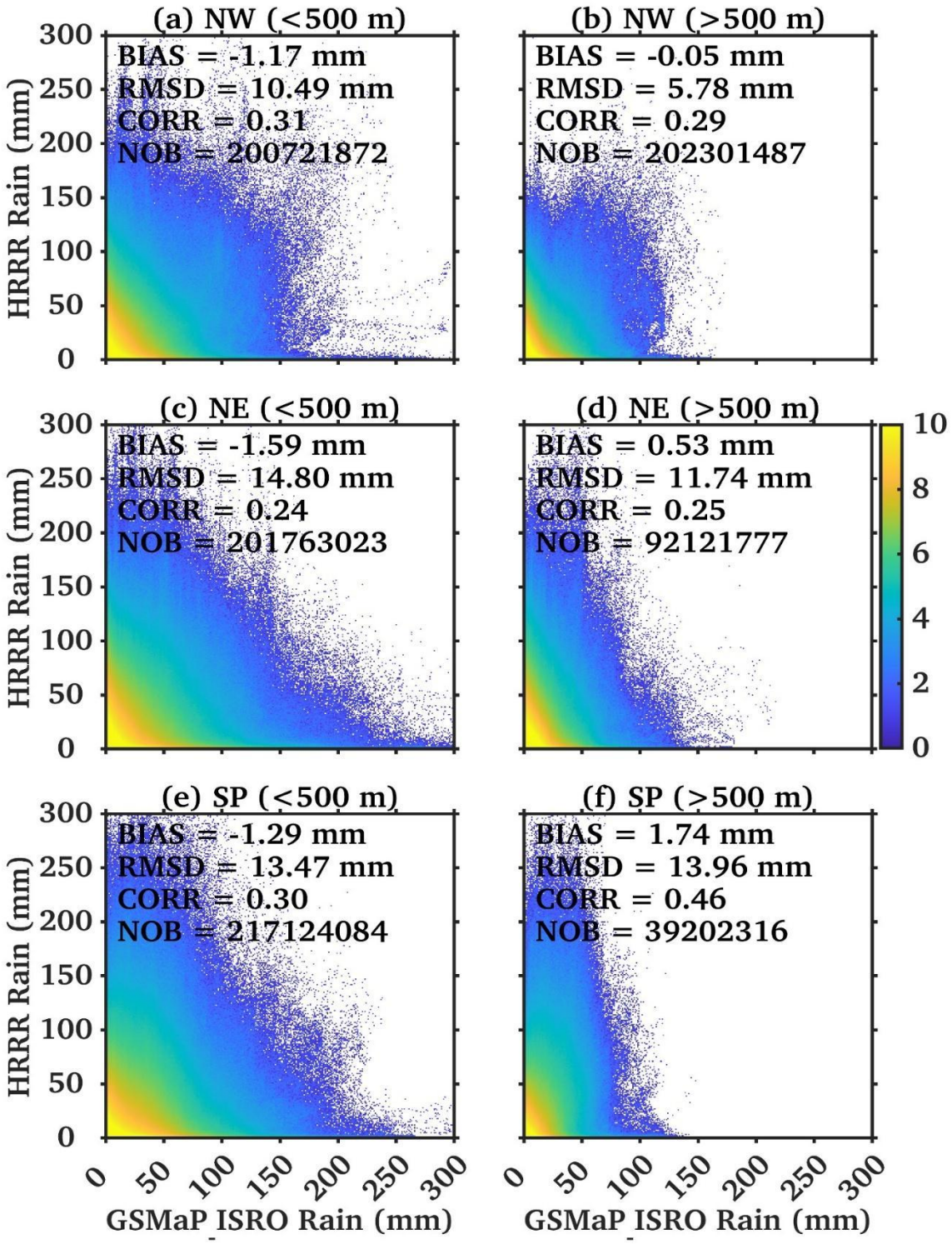


Fig. 8. Terrain-wise IMD-HRRR model rainfall forecast performance for different rainfall thresholds at 12-hour intervals.

Figures 7 & 8 indicate that IMD-HRRR rainfall skill varies systematically with terrain height and differs across the three domains. At the domain scale, the lowest terrain class contributes the largest number of cases, while higher-elevation bins are comparatively sparse, so the statistics at the upper terrain ranges should be interpreted with some caution. Even so, a clear pattern emerges: bias is generally negative in low terrain across all domains, suggesting a tendency for underestimation, whereas the sign and magnitude of bias become more heterogeneous in higher terrain. The RMSD increases notably in the NE and SP domains over elevated terrain, implying that forecast errors increase with topographic complexity. Correlation remains modest overall, but it is relatively stronger in the SP domain, particularly at terrain heights above 500 m, indicating better rain-rate association there than in the NW and NE domains. The paired scatter plots reinforce this message: low-terrain cases show a dense cluster at low rainfall amounts with substantial spread at higher intensities, while high-terrain cases retain some skill but also exhibit larger dispersion and domain-dependent bias behaviour. Overall, the results suggest that terrain exerts a meaningful control on HRRR performance, with elevated terrain amplifying forecast uncertainty and altering the bias structure, although the SP domain appears to retain comparatively better correspondence with GSMaP-ISRO rainfall in higher terrain.

An object-based spatial verification CRA was conducted across NW, NE, and SP IMD-HRRR model domains for four different 12-hour precipitation thresholds (50 mm/12 hours, 100 mm/12 hours, 150 mm/12 hours & 200 mm/12 hours). Table 3 below presents the domain-averaged spatial verification parameters, object displacement vectors, and complete Mean Square Error (MSE) error decompositions.

Table 3: CRA Table

Domain	Threshold (mm/12-hr)	Mean CSI	Mean Displacement	MSEdisp	MSEvol	MSE pattern
NW	50	0.0138	328.73	28.73	1.69×10^{-20}	75.2
NW	100	0.0083	354.6	28.73	1.69×10^{-20}	75.2
NW	150	0.005	377.43	28.73	1.69×10^{-20}	75.2
NW	200	0.0044	351.66	28.73	2.74×10^{-14}	75.2
NE	50	0.0182	294.26	60.29	7.19×10^{-20}	184.3

NE	100	0.0104	280.77	60.29	7.19×10^{-20}	184.3
NE	150	0.0057	305.62	60.29	7.19×10^{-20}	184.3
NE	200	0.0043	354.22	60.29	7.19×10^{-20}	184.3
SP	50	0.0183	312.77	80.85	$1.38\times^{10-19}$	206.92
SP	100	0.0043	368.39	80.85	$1.38\times^{10-19}$	206.92
SP	150	0.0011	400.17	80.85	$1.38\times^{10-19}$	206.92
SP	200	0.0003	449.16	80.85	1.38×10^{-19}	206.92

Figure 9(A) shows the non-linear decay of CSI for increasing thresholds of rainfall per 12 hours. As rainfall intensity thresholds increase from 50 mm to 200 mm per 12 hours, the categorical CSI rates experience steep non-linear decay across all domains. In the SP domain, mean CSI falls by 98.6% (from 0.0183 at 50 mm to 0.0003 at 200 mm). In the NE domain, mean CSI decreases by 76.4% (from 0.0182 to 0.0043), & in the NW domain, mean CSI decreases by 68.1% (from 0.0138 to 0.0044). These results highlight the classical double penalty challenge seen due to grid verification without considering the shifting/displacement of the deep convective cores at high precipitation thresholds. However, Figure 9(B) shows that the spatial mismatch between observed and forecast rain object centroids expands systematically at higher intensity limits. In the SP domain, average object displacement expands from 312.77 km at 50mm to 449.16 km at 200mm (+43.6%). In the NE domain, object displacement increases from 294.26 km at 50mm to 354.22 km at 200mm (+20.4%). In the NW domain, displacement peaks at 377.43 km at the 150mm threshold. So it can be seen that there is incongruence between the drop in CSI and the expansion of centroid spatial displacement vectors across different rainfall intensity thresholds.

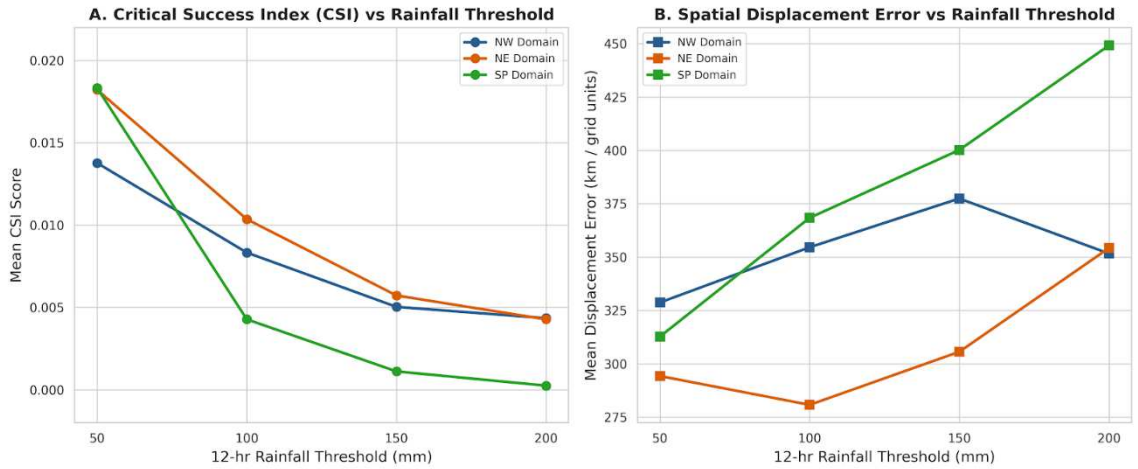


Fig. 9. (A) Threshold-wise IMD-HRRR model Critical Success Index for three domains and (B) Threshold-wise Spatial Displacement Error Growth from CRA.

Figure 10 shows the decomposition of the total errors in terms of displacement error, pattern error, and volume error. It shows a very consistent structural scenario in all three domains. The volume error across all domains and thresholds is negligible, with a mean bias ratio of about 1. This implies that the model condenses and converts the moisture into rainfall across the contiguous domain. The internal pattern or shape mismatch is seen to be the highest contributor to the total error. It shows a 72.4% error contribution in the NW domain, a 75.3% error contribution in the NE domain, and a 71.9% error contribution in the SP domain. The model fails to capture the fine-scale internal gradients and morphology of the intense convective cores even when the spatial location shifts are compensated. Displacement error contributes to about 27.6% of the errors in the NW domain, 24.7% in the NE domain, and 28.1% in the SP domain.

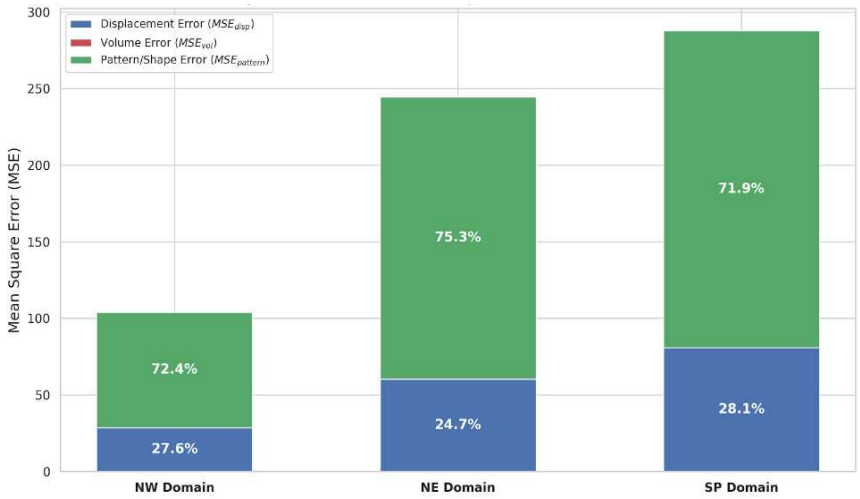


Fig. 10: Percentage share between displacement, volume, and pattern errors across the three IMD-HRRR domains.

Therefore, the mathematical decomposition of the total mean square error indicates an important aspect of decoupling between the volumetric mass conservation and spatial organisation of the rainfall system. The volume error remained negligible in all three domains for all the rainfall thresholds, suggesting skilled functioning of model microphysics capturing the moisture convergence scenario leading to the conservation of the total rainwater budget over isolated storms. However, the total forecast error is dominated by the spatial pattern error of 72.4% in NW, 75.3% in NE, and 71.9% in SP domains. The displacement error contributes to the majority of the remaining errors, from 24.7%, 27.6%, and 28.1% in the NE, NW, and SP domains, respectively. The results demonstrate that the IMD-HRRR forecast degradation during extreme precipitation events is mainly due to the macroscale steering flow leading to displacement errors and mismatch in microscale convective organisation leading to pattern and shape errors. The under- and overprediction of total rainfall volume have a relatively negligible contribution to the forecast degradation during extreme precipitation events.

4. Conclusion

This study looks at how skilful the IMD-HRRR model is at predicting extremely heavy rainfall (greater than 204.4 mm/day) across mainland India in 2023. The study relies on high-resolution satellite-gauge merged observations (GSMaP_ISRO) alongside traditional grid-based metrics, EDS, terrain-binned stratification, and spatial feature-orientated CRA object verification to get a full picture of where the model holds up and where it breaks down structurally.

IMD-HRRR reproduces the main synoptic features and regional precipitation belts of extreme events across all three operational domains, and it reliably picks up peak convective activity over the hazard-prone zones, which include the Assam–Meghalaya plateau, the Western Ghats, and the Konkan–Karnataka coastal belt. But the standard spatial metrics expose some localised biases underneath that success and indicate a dry bias over the Western Himalayan region and Kutch and a wet bias along the Western Ghats. Domain-averaged 12-hour rainfall predictions run persistently dry, from -0.61 mm in the NW to -0.93 mm in the NE, and RMSD is seen up to 1.79 mm in the NW and 3.54 mm in both the NE and SP. The usual categorical metric, CSI, falls off steeply as thresholds move into the 150–200 mm/12-hr range, largely due to a grid-point mismatch and "double penalty" problem. EDS tells a more encouraging story that the model discriminates meaningfully between rare, high-impact events even at those thresholds. NW shows best extreme-event skill as rainfall thresholds climb, while NE degrades faster past the 100 mm/12-hr mark.

Elevation influences the models' forecast accuracy. Low-terrain areas (under 100 m) are systematically underestimated across every domain, and in elevated terrain (above 500 m), topographic complexity widens the forecast dispersion and increases RMSD. The SP domain maintains a comparatively strong correlation (r ~0.46–0.50) at higher elevations (500–2500 m)

relative to the northern domains. This indicates that the model is able to capture terrain-forced orographic flow along the Western Ghats. The CRA error decomposition suggests that the degradation in extreme rainfall forecasts comes down to spatial positioning and convective organisation and is not due to water mass bias. Across every domain and threshold tested (50–200 mm/12-hr), the volume error component is negligible, which indicates that the IMD-HRRR parameterisations and data assimilation schemes are conserving the integrated moisture mass budget accurately over extreme storm entities. The total error budget is dominated by pattern and structural mismatch (71.9–75.3%), with centroid displacement making up the rest (24.7–28.1%).

The results show that IMD-HRRR gives skilled, high-resolution guidance for rapid-refresh early warning and disaster mitigation during extreme hydrometeorological events. Overcoming the structural limitation would require better microphysical parameterisations that can resolve the fine-scale gradients, intensity cores, and spatial morphology of deep convective cells more precisely. Data assimilation improvement would be required to better resolve low-level moisture convergence and steering flows, leading to improvement in the centroid displacement. And in the complex mountain regions like the Western Himalayas and the Northeast hills, better micro-scale topography and land-surface feedback representation will be key to managing elevation-dependent error growth.

Declarations

No funding was received for conducting this study. The authors have no relevant financial or non-financial interests to disclose.

Author's Contribution:

Akhil Srivastava: - Conceptualisation, Methodology, Software, Data curation; Investigation; Writing - draft, Writing - review & editing, Validation, Formal analysis.
Prashant Kumar: - Conceptualisation; Methodology; Software; Investigation; Writing - review & editing; Validation; Formal analysis.
Raghvendra Raju Nadimpalli: - Methodology, Writing - review & editing; Validation.
Amit Kumar: - Software, Validation, Investigation.
C. J. Johny: - data Curation; Experiment; Software.
Ananda Kumar Das: - Supervision.
Pradeep Kumar Thapliyal:- Supervision.

References

Agnihotri, G., Gouda, K. C., & Das, S. (2021). Characteristics of pre-monsoon convective systems over south peninsular India and neighborhood using tropical rainfall measuring mission's precipitation radar. Meteorology and Atmospheric Physics, 133(2), 193-203.

Ali, H., Peleg, N., & Fowler, H. J. (2021). Global scaling of rainfall with dewpoint temperature reveals considerable ocean-land difference. Geophysical Research Letters, 48(15), e2021GL093798.

Ashrit, R., & Mohandas, S. (2010). Mesoscale model forecast verification during monsoon 2008. Journal of Earth System Science, 119(4), 417-446.

Ashrit, R., Sharma, K., Dube, A., Iyengar, G., Mitra, A., & Rajagopal, E. N. (2015). Verification of short range forecasts of extreme rainfall during monsoon. Mausam, 66(3), 375-386.

Das, S., Ashrit, R., Iyengar, G. R., Mohandas, S., Das Gupta, M., George, J. P., ... & Dutta, S. K. (2008). Skills of different mesoscale models over Indian region during monsoon season: Forecast errors. Journal of earth system science, 117(5), 603-620.

Das, S., Sarkar, A., Das, M. K., Rahman, M. M., & Islam, M. N. (2015). Composite characteristics of Nor'westers based on observations and simulations. Atmospheric research, 158, 158-178.

Durai, V. R., & Bhardwaj, R. (2013). Improving precipitation forecasts skill over India using a multi-model ensemble technique. Geofizika, 30(2), 155-172.

Fowler, H. J., Lenderink, G., Prein, A. F., Westra, S., Allan, R. P., Ban, N., ... & Zhang, X. (2021). Anthropogenic intensification of short-duration rainfall extremes. Nature Reviews Earth & Environment, 2(2), 107-122.

Fowler, H. J., Wasko, C., & Prein, A. F. (2021). Intensification of short-duration rainfall extremes and implications for flood risk: Current state of the art and future directions. Philosophical transactions. Series A, Mathematical, physical, and engineering sciences, 379(2195), 20190541.

Fowler, H. J., Wasko, C., & Prein, A. F. (2021). Intensification of short-duration rainfall extremes and implications for flood risk: Current state of the art and future directions. Philosophical transactions. Series A, Mathematical, physical, and engineering sciences, 379(2195), 20190541.

Goswami, B. N., Venugopal, V., Sengupta, D., Madhusoodanan, M. S., & Xavier, P. K. (2006). Increasing trend of extreme rain events over India in a warming environment. Science, 314(5804), 1442-1445.

Guhathakurta, P., & Rajeevan, M. (2008). Trends in the rainfall pattern over India. International Journal of Climatology: A Journal of the Royal Meteorological Society, 28(11), 1453-1469.

Jolliffe, I. T., & Stephenson, D. B. (Eds.). (2012). Forecast verification. Oxford: Wiley.

Kalnay, E., Lord, S. J., & McPherson, R. D. (1998). Maturity of operational numerical weather prediction: Medium range. Bulletin of the American Meteorological Society, 79(12), 2753-2770.

Kubota, T., Aonashi, K., Ushio, T., Shige, S., Takayabu, Y. N., Kachi, M., ... & Oki, R. (2020). Global Satellite Mapping of Precipitation (GSMaP) products in the GPM era. In Satellite precipitation measurement: Volume 1 (pp. 355-373). Cham: Springer International Publishing.

Kumar, P., Gairola, R., Kubota, T., & Kishtawal, C. (2021). Hybrid assimilation of satellite rainfall product with high density gauge network to improve daily estimation: A case of Karnataka, India. Journal of the Meteorological Society of Japan. Ser. II, 99(3), 741-763.

Kumar, P., Srivastava, S. S., Jivani, N., Varma, A. K., Yokoyama, C., & Kubota, T. (2024). Long-term assessment of ERA5 reanalysis rainfall for lightning events over India observed by tropical rainfall measurement mission lightning imaging sensor. Quarterly Journal of the Royal Meteorological Society, 150(761), 2472-2488.

Kumar, P., Varma, A. K., Kubota, T., Yamaji, M., Tashima, T., Mega, T., & Ushio, T. (2022). Long-term high-resolution gauge adjusted satellite rainfall product over India. Earth and Space Science, 9(12), e2022EA002595.

Kumar, S., & Bhat, G. S. (2016). Vertical profiles of radar reflectivity factor in intense convective clouds in the tropics. Journal of Applied Meteorology and Climatology, 55(5), 1277-1286.

Lenderink, G., Barbero, R., Loriaux, J. M., & Fowler, H. J. (2017). Super-Clausius–Clapeyron scaling of extreme hourly convective precipitation and its relation to large-scale atmospheric conditions. Journal of Climate, 30(15), 6037-6052.

Lenderink, G., de Vries, H., Fowler, H. J., Barbero, R., van Ulft, B., & Van Meijgaard, E. (2021). Scaling and responses of extreme hourly precipitation in three climate experiments with a convection-permitting model. Philosophical transactions. Series A, Mathematical, physical, and engineering sciences, 379(2195), 20190544.

Magnusson, L., & Källén, E. (2013). Factors influencing skill improvements in the ECMWF forecasting system. Monthly Weather Review, 141(9), 3142-3153.

Mandal, V., De, U. K., & Basu, B. K. (2007). Precipitation forecast verification of the Indian summer monsoon with intercomparison of three diverse regions. Weather and forecasting, 22(3), 428-443.

Mega, T., Ushio, T., Kubota, T., Kachi, M., Aonashi, K., & Shige, S. (2014, August). Gauge adjusted global satellite mapping of precipitation (GSMaP_Gauge). In 2014 XXXIth URSI General Assembly and Scientific Symposium (URSI GASS) (pp. 1-4). IEEE.

Naidu, C. V., Raju, A. D., Satyanarayana, G. C., Kumar, P. V., Chiranjeevi, G., & Suchitra, P. (2015). An observational evidence of decrease in Indian summer monsoon rainfall in the recent three decades of global warming era. Global and Planetary Change, 127, 91-102.

Paegle, J., Pielke, R. A., Dalu, G. A., Miller, W., Garratt, J. R., Vukicevic, T., ... & Nicolini, M. (1990). Predictability of flows over complex terrain. In Atmospheric Processes over Complex Terrain (pp. 285-299). Boston, MA: American Meteorological Society.

Parthasarathy, B., Munot, A. A., & Kothawale, D. R. (1994). All-India monthly and seasonal rainfall series: 1871–1993. Theoretical and Applied Climatology, 49(4), 217-224.

Revadekar, J. V., & Preethi, B. (2012). Statistical analysis of the relationship between summer monsoon precipitation extremes and foodgrain yield over India. International Journal of Climatology, 32(3), 419-429.

Roxy, M. K., Ghosh, S., Pathak, A., Athulya, R., Mujumdar, M., Murtugudde, R., ... & Rajeevan, M. (2017). A threefold rise in widespread extreme rain events over central India. Nature communications, 8(1), 708.

Samantray, P., & Gouda, K. C. (2024). A review on the extreme rainfall studies in India. Natural Hazards Research, 4(3), 347-356.

Sen Roy, S., & Balling Jr, R. C. (2004). Trends in extreme daily precipitation indices in India. International Journal of Climatology: A Journal of the Royal Meteorological Society, 24(4), 457-466.

Sharma, K., Ashrit, R., Bhatla, R., Rakhi, R., Iyengar, G. R., & Rajagopal, E. N. (2017). Verification of heavy rainfall in NWP models: A case study. Mausam, 68(4), 699-712.

Siddique, R., Mejia, A., Brown, J., Reed, S., & Ahnert, P. (2015). Verification of precipitation forecasts from two numerical weather prediction models in the Middle Atlantic Region of the USA: A precursory analysis to hydrologic forecasting. Journal of Hydrology, 529, 1390-1406.

Srivastava, A., Kumar, P., Panda, S. K., Das, A. K., Pattanaik, D. R., & Mohapatra, M. (2024). Development of India Meteorological Department: High Resolution Rapid Refresh (IMD-HRRR) Modeling System for Very Short Range Weather Forecasting: A. Srivastava et al. Pure and Applied Geophysics, 181(11), 3393-3408.

Stephenson, D. B., Casati, B., Ferro, C. A. T., & Wilson, C. A. (2008). The extreme dependency score: A non-vanishing measure for forecasts of rare events. Meteorological Applications: A journal of forecasting, practical applications, training techniques and modelling, 15(1), 41-50.

Turner, A. G., & Annamalai, H. (2012). Climate change and the South Asian summer monsoon. Nature Climate Change, 2(8), 587-595.

Vitart, F. (2013). Evolution of ECMWF sub-seasonal forecast skill scores over the past 10 years. ECMWF.

Walters, D., Wood, N., Vosper, S., Milton, S., Bysouth, C., Earnshaw, P., ... & Roberts, M. (2014). ENDGame: A new dynamical core for seamless atmospheric prediction. Met Office Rep.

Wang, S., & Yuan, X. (2018). Extending seasonal predictability of Yangtze River summer floods. Hydrology and Earth System Sciences, 22(8), 4201-4211.

Wilks, D. S., & Wilks, D. S. (2006). Statistical methods in the atmospheric sciences (Vol. 627). London: Academic press.